

1 **Global assessment of how averaging over spatial heterogeneity in precipitation and potential evapotranspiration**  
2 **affects modeled evapotranspiration rates**

3

4 Elham Rouholahnejad Freund<sup>1,2</sup>, Ying Fan<sup>3</sup>, James W. Kirchner<sup>2,4,5</sup>

5

6 <sup>1</sup>Laboratory of Hydrology and Water Management, Ghent University, Ghent, Belgium

7 <sup>2</sup>Department of Environmental Systems Science, ETH Zurich, 8092, Zurich, Switzerland

8 <sup>3</sup>Department of Earth and Planetary Sciences, Rutgers University, New Brunswick, NJ, United States

9 <sup>4</sup>Swiss Federal Research Institute WSL, Birmensdorf, 8903, Switzerland

10 <sup>5</sup>Dept. of Earth and Planetary Science, University of California, Berkeley, CA 94720, United States

11

12 *Correspondence to:* Elham Rouholahnejad Freund, elham.rouholahnejad@gmail.com

13

14 **Short summary**

15 Evapotranspiration (ET) rates and the properties that regulate them are spatially heterogeneous. Averaging over  
16 spatial heterogeneity in precipitation and potential evapotranspiration as main drivers of ET may lead to biased  
17 estimates of energy and water fluxes from the land surface to the atmosphere. Here we show that this bias will be  
18 largest in mountainous terrain, in regions with temperate climates and dry summers, and in landscapes where  
19 spatial variations in precipitation and potential evapotranspiration are inversely correlated.

20

21 **Abstract**

22 The major goal of large-scale Earth System Models (ESMs) is to understand and predict global change. However,  
23 computational constraints require ESMs to operate on relatively large spatial grids (typically ~1 degree or ~100 km  
24 in size), with the result that the heterogeneity in land surface properties and processes at smaller spatial scales  
25 cannot be explicitly represented. Averaging over this spatial heterogeneity may lead to biased estimates of energy  
26 and water fluxes. Here we estimate how averaging over spatial heterogeneity in precipitation (P) and potential  
27 evapotranspiration (PET) may affect grid-cell-averaged evapotranspiration (ET) rates, as seen from the atmosphere  
28 over heterogeneous landscapes across the globe. Our goal is to identify where, under what conditions, and at what  
29 scales this heterogeneity bias could be most important, but not to quantify its absolute magnitude. We use Budyko  
30 curves as simple functions that relate ET to precipitation (P) and potential evapotranspiration (PET). Because the  
31 relationships driving ET are nonlinear, averaging over sub-grid heterogeneity in P and PET will lead to biased  
32 estimates of average ET. We examine the global distribution of this bias, its scale dependence, and its sensitivity to  
33 variations in P versus PET. Our analysis shows that this "heterogeneity bias" is more pronounced in mountainous  
34 terrain, in landscapes where spatial variations in P and PET are inversely correlated, and in regions with temperate  
35 climates and dry summers. We also show that this heterogeneity bias increases on average, and expands over  
36 larger areas, as the grid cell size increases. Our work outlines a strategy for quantifying heterogeneity biases and  
37 potentially correcting for them, and highlights regions where more detailed mechanistic modeling is needed.

38

39

## 40 1. Introduction

41 Earth System Models (ESMs) are designed to understand interactions between the land surface, atmosphere, and  
42 oceans and to predict global environmental changes. However, the Earth system and its underlying physical  
43 processes are highly heterogeneous across orders of magnitude in scale below the scale of typical ESM grids (e.g.,  
44 1° by 1°). Despite increasing recognition of the need to mechanistically represent physical processes in ESMs,  
45 currently even the most disaggregated large-scale ESMs cannot explicitly represent the spatial heterogeneity of  
46 land surface hydrological properties at scales that are important to atmospheric fluxes. Averaging over land surface  
47 properties at the scale of ESM model grid cells may have important implications for water and energy flux estimates  
48 (Avisar and Pielke, 1989; Giorgi and Avisar, 1997; Ershadi et al., 2013; Lu et al., 2014).

49  
50 Estimates of evapotranspiration (ET) fluxes have significant implications for future temperature predictions. Smaller  
51 ET fluxes imply greater sensible heat fluxes and, therefore, drier and warmer conditions in the context of climate  
52 change (Seneviratne et al., 2010). Surface evaporative fluxes (and thus energy partitioning over land surfaces) are  
53 nonlinear functions of available water and energy, and thus are coupled to spatially heterogeneous surface  
54 characteristics (e.g., soil type, vegetation, topography) and meteorological inputs (e.g., radiative flux, wind, and  
55 precipitation; Kalma et al., 2008; Sharaeeni and Or, 2010; Holland et al., 2013). These characteristics are spatially  
56 variable on length scales of <1 m to many kilometers, well below typical ESM grid scales of ~100 km. ESMs calculate  
57 grid-averaged surface and atmospheric fluxes using parameterizations that correspond to grid-averaged properties  
58 of the land surface (Sato et al., 1989; Koster et al., 2006; Santanello and Peters-Lidard, 2011). Thus ET estimates  
59 that are derived from spatially-averaged land surface properties do not capture ET variations driven by the  
60 underlying surface heterogeneity (McCabe and Wood, 2006). Because the relationships driving ET are nonlinear,  
61 the average ET flux from a heterogeneous landscape may be different from an ET estimate calculated from spatially  
62 averaged inputs (Rouholahnejad Freund and Kirchner, 2017).

63  
64 Several studies have quantified the effects of land surface heterogeneity on potential evapotranspiration (PET) and  
65 latent heat (LH) fluxes, and have found that averaging over land surface heterogeneity can potentially bias ET  
66 estimates either positively or negatively. For example, Boone and Wetzel (1998) studied the effects of soil texture  
67 variability within each pixel in the Land-Atmosphere-Cloud Exchange (PLACE) model, which has a spatial resolution  
68 of approximately 100 by 100 km. They reported that accounting for sub-grid variability in soil texture reduced  
69 global ET by 17%, increased total runoff by 48%, and increased soil wetness by 19%, compared to using a  
70 homogenous soil texture to describe the entire grid cell. Kollet (2009) found that heterogeneity in soil hydraulic  
71 conductivity had a strong influence on evapotranspiration during the dry months of the year, but not during  
72 months with sufficient moisture availability. Hong et al. (2009) reported that aggregating radiance data from 30 m  
73 to 60, 120, 250, 500, and 1000 m resolution (input upscaling) and then calculating ET from these aggregated inputs  
74 at these grid scales using Surface Energy Balance Algorithm for Land (SEBAL, Bastiaanssen et al., 1998a) yields  
75 slightly larger ET estimates as compared to ET calculated with finer resolution inputs and then aggregated at the

76 desired grid scales (output upscaling). The discrepancy between ET estimated with the output upscaling method  
77 and the input upscaling method grows as the size of the grid cell increases (the difference between ET calculated  
78 from the input and output upscaling methods is ~20% more at a grid scale of 1 km by 1 km compared to a grid scale  
79 of 120 m by 120 m). Aminzadeh et al. (2017) investigated the effects of averaging surface heterogeneity and soil  
80 moisture availability on potential evaporation from a heterogeneous land surface including bare soil and vegetation  
81 patches. They found that if the heterogeneity length scale is smaller than the convective atmospheric boundary  
82 layer (ABL) thickness, averaging over heterogeneous land surfaces has only a small effect on average potential  
83 evaporation rates. Averaging over larger-scale heterogeneities, however, led to overestimates of potential  
84 evaporation.

85  
86 Heterogeneity biases have also been identified in ET calculation algorithms that use remote sensing data as inputs.  
87 McCabe and Wood (2006) found that remote sensing retrievals of ET are larger than the corresponding in-situ flux  
88 estimates and characterized the roles of land surface heterogeneity and remote sensing resolution in the retrieval  
89 of evaporative flux. McCabe and Wood (2006) used Landsat (60 m), Advanced Space borne Thermal Emission and  
90 Reflection Radiometer (ASTER) (90 m), and MODIS (1020 m) independently to estimate ET over the Walnut Creek  
91 watershed in Iowa. They compared these remote sensing estimates to eddy covariance flux measurements and  
92 reported that Landsat and ASTER ET estimates had a higher degree of consistency with one another and correlated  
93 better to the ground measurements (0.87 and 0.81, respectively) than MODIS- based ET estimates did. All three  
94 remote sensing products overestimated ET as compared to ground measurements (at 12 out of 14 tower sites).  
95 Upon aggregation of Landsat and ASTER retrievals to MODIS scale (1 km), the correlation with the ground  
96 measurements decreased to 0.75 and 0.63 for Landsat and ASTER, respectively.

97  
98 Contrary to overestimation bias, many remotely sensed ET estimates that include parameters related to  
99 aerodynamic resistance are significantly affected by heterogeneity, and underestimate ET as the scale increases  
100 (Ershadi et al., 2013). Because aerodynamic resistance is significantly affected by land surface properties (e.g.,  
101 vegetation height, roughness length, and displacement height), decreases in aerodynamic resistance at coarser  
102 resolutions could lead to smaller estimates of evapotranspiration. Ershadi et al. (2013) showed that input  
103 aggregation from 120m to 960 m in Surface Energy Balance System (SEBS, Su, 2002) leads to up to 15 %  
104 underestimation of ET at the larger grid resolution in a study area in the south-east of Australia.  
105 Rouholahnejad Freund and Kirchner (2017) quantified the impact of sub-grid heterogeneity on grid-average ET  
106 using a simple Budyko curve (Turc, 1954; Mezentsev, 1955) in which long-term average ET is a non-linear function  
107 of long-term averages of precipitation (P) and potential evaporation (PET). They showed mathematically that  
108 averaging over spatially heterogeneous P and PET results in overestimation of ET within the Budyko framework (Fig.  
109 1). Their analysis implies that large-scale ESMs that overlook land surface heterogeneity will also yield biased  
110 evapotranspiration estimates due to the inherent nonlinearity in ET processes. They did not, however, determine  
111 where around the globe, and under what conditions, this heterogeneity bias is likely to be most important.

112

113 The recognition that spatial averaging can potentially lead to biased flux estimates has prompted methods for  
114 representing sub-grid-scale heterogeneities and processes within ESMs. Accounting for land surface heterogeneity  
115 in large-scale ESMs is not merely constrained by limitations in both computational power (Baker et al. 2017) and  
116 the availability of high-resolution forcing data, but also by the fact that the atmospheric and land surface  
117 components of some ESMs operate at different resolutions. There have been several attempts to integrate sub-grid  
118 heterogeneity in ESMs while keeping the computational costs affordable. In “mosaic” approaches, the model is run  
119 separately for each surface type in a grid cell, and then the surface-specific fluxes are area-weighted to calculate  
120 the grid-cell average fluxes (e.g., Avissar and Pielke, 1989; Koster and Suarez, 1992). The “effective parameter”  
121 approach (e.g., Wood and Mason, 1991; Mahrt et al., 1992), by contrast, seeks to estimate effective parameter  
122 values at the grid cell scale that subsume the effects of sub-grid heterogeneity. Estimating these effective  
123 parameters can be challenging because the relevant land-surface processes typically depend nonlinearly on  
124 multiple interacting parameters, and land-surface signals at different scales are propagated and diffused differently  
125 in the atmosphere. Alternatively, the “correction factor” approach (e.g., Maayar and Chen, 2006) uses sub-grid  
126 information on spatially heterogeneous land-surface processes and properties to estimate multiplicative correction  
127 factors for fluxes that are originally calculated from spatially averaged inputs at the grid-cell scale. All three  
128 approaches try to reduce the heterogeneous problem to a homogeneous one that has equivalent effects on the  
129 atmosphere at the grid-cell scale.

130

131 There is a growing need to understand how sub-grid heterogeneity (and the atmosphere’s integration of it) affect  
132 grid-scale water and energy fluxes, and to develop effective methods to incorporate these effects in ESMs (Clark et  
133 al., 2015, Fan et al., 2019). In a previous study, we proposed a general framework for quantifying systematic biases  
134 in ET estimates due to averaging over heterogeneities (Rouholahnejad Freund and Kirchner, 2017). We used the  
135 Budyko framework as a simple estimator of ET, and demonstrated theoretically how averaging over heterogeneous  
136 precipitation and potential evapotranspiration can lead to systematic overestimation of long-term average ET  
137 fluxes from heterogeneous landscapes. In the present study, we apply this analysis across the globe and highlight  
138 the locations where the heterogeneity bias is largest. Our hypotheses, derived from the Budyko framework as  
139 summarized in Eq. (4) below, are that (1) strongly heterogeneous landscapes, such as mountainous terrain, will  
140 exhibit greater heterogeneity bias, (2) this bias will be larger in climates where P and PET are inversely correlated in  
141 space, and (3) heterogeneity bias will decrease as the spatial scales of averaging decrease.

142

## 143 **2. Effects of sub-grid heterogeneity on ET estimates in the Budyko framework**

144 Budyko (1974) showed that long-term annual average evapotranspiration is a function of both the supply of water  
145 (precipitation, P) and the evaporative demand (potential evapotranspiration, PET) under steady-state conditions  
146 and in catchments with negligible changes in storage (Eq. 1; Turc, 1954; Mezentsev, 1955):

147

$$ET = f(P, PET) = \frac{P}{\left(\left(\frac{P}{PET}\right)^n + 1\right)^{1/n}}. \quad (1)$$

148 where ET is actual evapotranspiration, P is precipitation, PET is potential evaporation, and n (dimensionless) is a  
149 catchment-specific parameter that modifies the partitioning of P between ET and discharge.

150  
151 Evapotranspiration rates are inherently bounded by energy and water limits. Under arid conditions ET is limited by  
152 the available supply of water (the water limit line in Fig. 1b), while under humid conditions ET is limited by  
153 atmospheric demand (PET) and converges toward PET (the energy limit line in Fig. 1b). Budyko showed that over a  
154 long period and under steady-state conditions, hydrological systems function close to their energy or water limits.  
155 These intrinsic water and energy constraints make the Budyko curve downward-curving.

156  
157 In a heterogeneous landscape, like the simple example of two model columns in Fig. 1a, P and PET vary spatially.  
158 The two columns with heterogeneous P and PET are represented by the two solid black circles on the Budyko curve  
159 in Fig. 1b. In this hypothetical two-column example, the true average of ET values calculated from individual  
160 heterogeneous inputs (the solid black circles) lies below the curve (the grey circle, labeled "true average").  
161 However, if we aggregate the two columns and consider the system as one column with average properties, the  
162 function of average inputs (averaged P and PET over the two columns) lies on the Budyko curve (the open circle)  
163 which is larger than the true average of the two columns. In short, in any downward curving function, the function  
164 of the average inputs (the open circle) will always be larger than the average of the individual function values (the  
165 true average; grey circle). The difference between the two can be termed the "heterogeneity bias".

166  
167 In a previous study (Rouholahnejad Freund and Kirchner, 2017) we showed that when nonlinear underlying  
168 relationships are used to predict average behaviour from averaged properties, the magnitude of the resulting  
169 heterogeneity bias can be estimated from the degree of the curvature in the underlying function and the range  
170 spanned by the individual data being averaged. Here we summarize these findings as building blocks of the current  
171 study. The second-order, second-moment Taylor expansion of the ET function  $f(P, PET)$  (Eq. 1) around its mean  
172 directly yields:

$$173 \quad \bar{f}(P, PET) = \overline{ET} \approx f(\bar{P}, \overline{PET}) + \frac{1}{2} \frac{\partial^2 f}{\partial P^2} var(P) + \frac{1}{2} \frac{\partial^2 f}{\partial PET^2} var(PET) + \frac{\partial^2 f}{\partial P \partial PET} cov(P, PET) \quad , \quad (2)$$

174 where  $\bar{f}(P, PET)$  is the true average of the spatially heterogeneous ET function,  $f(\bar{P}, \overline{PET})$  is the ET function  
175 evaluated at its average inputs  $\bar{P}$  and  $\overline{PET}$ , and the derivatives are calculated at  $\bar{P}$  and  $\overline{PET}$ . Evaluating the  
176 derivatives using Eq. (1) and reshuffling the terms, Rouholahnejad Freund and Kirchner (2017) obtained the  
177 following expression for the heterogeneity bias, the difference between the average ET,  $\bar{f}(P, PET)$ , and the ET  
178 function evaluated at the mean of its inputs,  $f(\bar{P}, \overline{PET})$ :

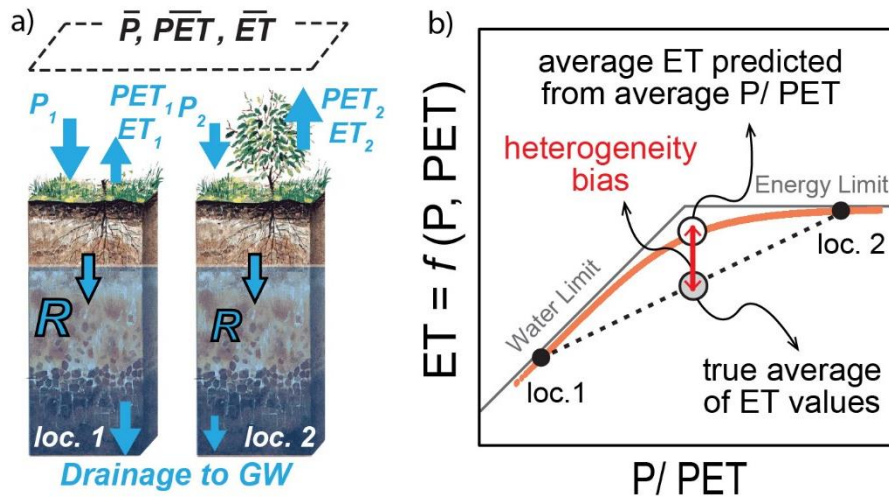
179 
$$f(\bar{P}, \overline{PET}) - \bar{f}(P, PET) \approx (n+1) \frac{\bar{P}^{n+1} \overline{PET}^{n+1}}{(\bar{P}^n + \overline{PET}^n)^{2+1/n}} \left[ \frac{1}{2} \frac{\text{var}(P)}{\bar{P}^2} + \frac{1}{2} \frac{\text{var}(PET)}{\overline{PET}^2} - \frac{\text{cov}(P, PET)}{\bar{P} \overline{PET}} \right]. \quad (3)$$

180 To more clearly show the effects of variations in P and PET, Eq. (3) can be reformulated as follows:

181 
$$(n+1) \frac{\bar{P}^{n+1} \overline{PET}^{n+1}}{(\bar{P}^n + \overline{PET}^n)^{2+1/n}} \left[ \frac{1}{2} \left( \frac{SD(P)}{\bar{P}} \right)^2 + \frac{1}{2} \left( \frac{SD(PET)}{\overline{PET}} \right)^2 - r_{P,PET} \left( \frac{SD(P)}{\bar{P}} \right) \left( \frac{SD(PET)}{\overline{PET}} \right) \right]. \quad (4)$$

182 Equation (4) shows that the heterogeneity bias depends on only four quantities: the fractional variation (i.e., the  
 183 coefficient of variation) in precipitation  $\left(\frac{SD(P)}{\bar{P}}\right)$  and in potential ET  $\left(\frac{SD(PET)}{\overline{PET}}\right)$ , the correlation between precipitation  
 184 and potential ET ( $r_{P,PET}$ ), and the function  $(n+1) \frac{\bar{P}^{n+1} \overline{PET}^{n+1}}{(\bar{P}^n + \overline{PET}^n)^{2+1/n}}$ , which quantifies the curvature in the ET function  
 185 in Budyko space. As shown by Fig. 1b and Eq. (2), the discrepancy between average of the ET function and the ET  
 186 function of the average inputs (the heterogeneity bias) is proportional to both the degree of nonlinearity in the  
 187 function, as defined by its second derivatives, and the variability of P and PET. Equation (4) allows one to estimate  
 188 how much the curvature of the ET function and the fractional variability (standard deviation divided by mean) of P  
 189 and PET will affect estimates of ET. However, to the best of our knowledge, the consequences of these  
 190 nonlinearities for global evaporative flux estimates have not previously been quantified.

191



192  
 193 Figure 1. Heterogeneity bias in a hypothetical two-column model in the Budyko framework. The true average ET of  
 194 the columns (gray circle) lies below the curve and is less than the average ET estimated from the average P/PET of  
 195 the two columns (open circle). The heterogeneity bias depends on the curvature of the function and the spread of  
 196 its inputs. Both panels are adapted from Rouholahnejad Freund and Kirchner (2017).

197

198 **3. Effects of sub-grid heterogeneity on ET estimates at 1° by 1° grid scale across the globe**

199 Across a landscape of similar size to a typical ESM grid cell ( $1^\circ$  by  $1^\circ$ ), soil moisture, atmospheric demand (PET) and  
200 precipitation (P) will vary with topographic position; hillslopes will typically be drier, and riparian regions will be  
201 wetter. To map the spatial pattern in the heterogeneity bias that results from averaging over this land surface  
202 heterogeneity, we applied the approach outlined in section 2 to the global land surface area at  $1^\circ$  by  $1^\circ$  grid scale.  
203 Within each  $1^\circ$  by  $1^\circ$  grid cell, we used 30 arc-second values of P (WorldClim; Hijmans et al., 2005) and PET  
204 (WorldClim; Hijmans et al., 2005) to examine the variations in small-scale climatic drivers of ET. Because 30 arc-  
205 seconds is nearly 1 km, hereafter we refer to the 30 arc-second data as 1km values for simplicity. The spatial  
206 distribution of long-term annual averages (1960-1990) of P and PET values at 1 km resolution, along with 1km  
207 values of the aridity index ( $AI=P/PET$ ), are shown in Fig 2a-c. ET values calculated from these 1km P and PET values  
208 using Eq. (1) are then averaged at  $1^\circ$  by  $1^\circ$  scale ("true average", Fig. 2e). We also averaged the 1km values of P and  
209 PET within each grid cell and then modeled ET using the Budyko curve (Eq. 1) applied to these averaged input  
210 values. The difference between these two ET estimates is the heterogeneity bias.

211

212 We also calculated the heterogeneity bias using Eq. (4), which describes how the nonlinearity in the governing  
213 equation and the heterogeneity in P and PET jointly contribute to the heterogeneity bias. The heterogeneity bias  
214 estimates obtained by Eq. (4) were functionally equivalent ( $R^2=0.97$ , root mean square error of 0.17%) to those  
215 obtained by direct calculation using Eq. (1) as described above.

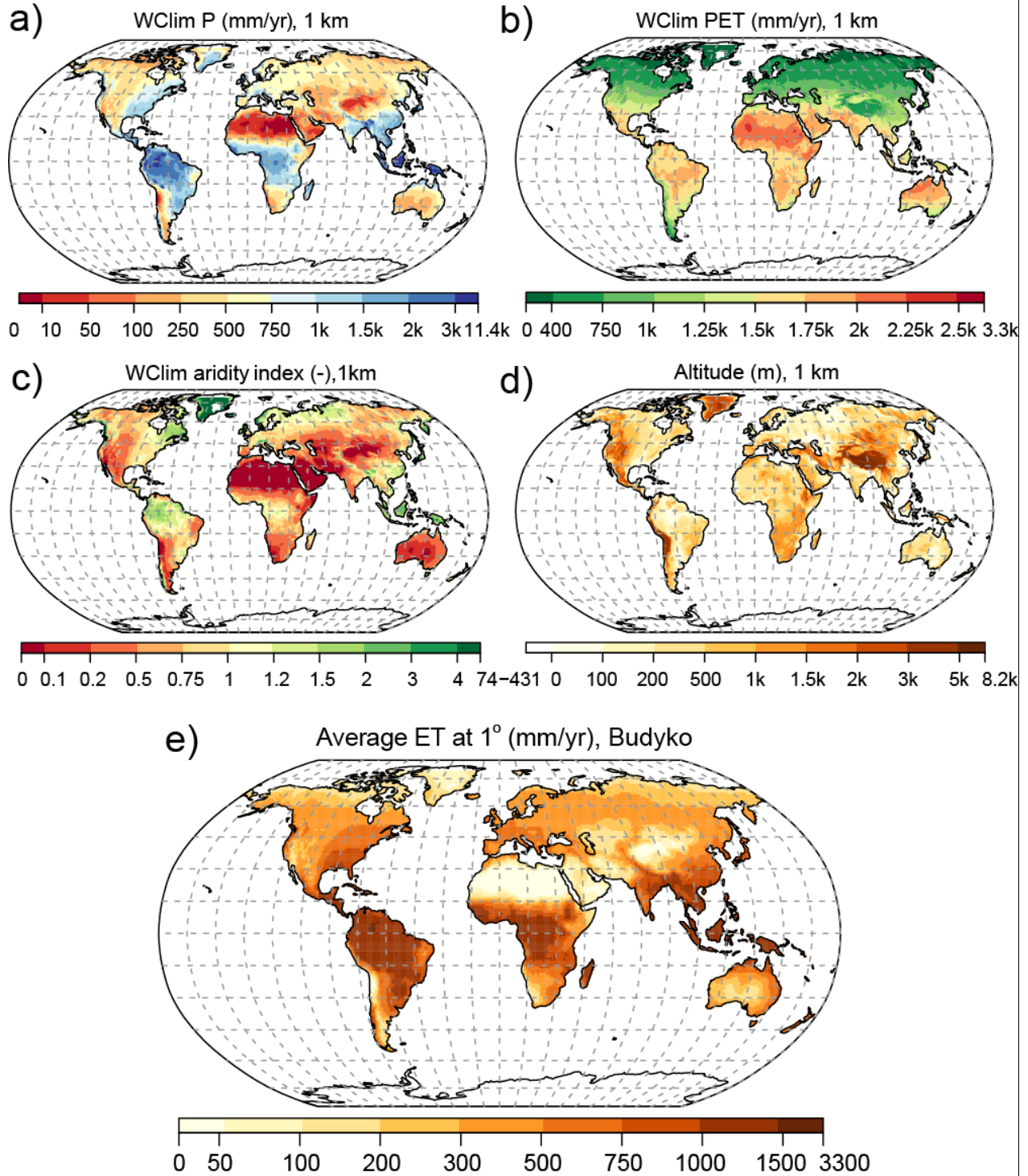
216

217 Fig. 3a-d illustrates the variability (quantified by standard deviation) of 1km values of P, PET, aridity index, and  
218 altitude at the  $1^\circ$  by  $1^\circ$  grid scale. The heterogeneity bias in long-term average ET fluxes at the  $1^\circ$  by  $1^\circ$  grid scale  
219 (Fig. 3e) highlights regions around the globe where ET fluxes are likely to be systematically overestimated. The  
220 spatial distribution of the heterogeneity bias calculated using Eq. 4 (Fig. 3e) closely coincides with locations where  
221 the aridity index is highly variable (Fig. 3c), which is driven in turn by topographic variability (Fig. 3d). Strongly  
222 heterogeneous landscapes exhibit significant heterogeneity biases in long-term average ET fluxes. Although the  
223 global average heterogeneity bias is small (<1%), physically based ET calculations may exhibit larger heterogeneity  
224 biases than the modest values we calculate here, because the Budyko approach already subsumes spatial  
225 heterogeneity effects at the catchment scale (and also temporal heterogeneity effects due to its steady-state  
226 assumptions). The heterogeneity biases in ET estimates shown in Fig. 3e correspond to long-term average ET  
227 estimates. Given the fact that P and PET can vary temporally (i.e., seasonality), the actual bias could be much larger,  
228 particularly where P and PET are inversely correlated (see the last term of Eq. 4).

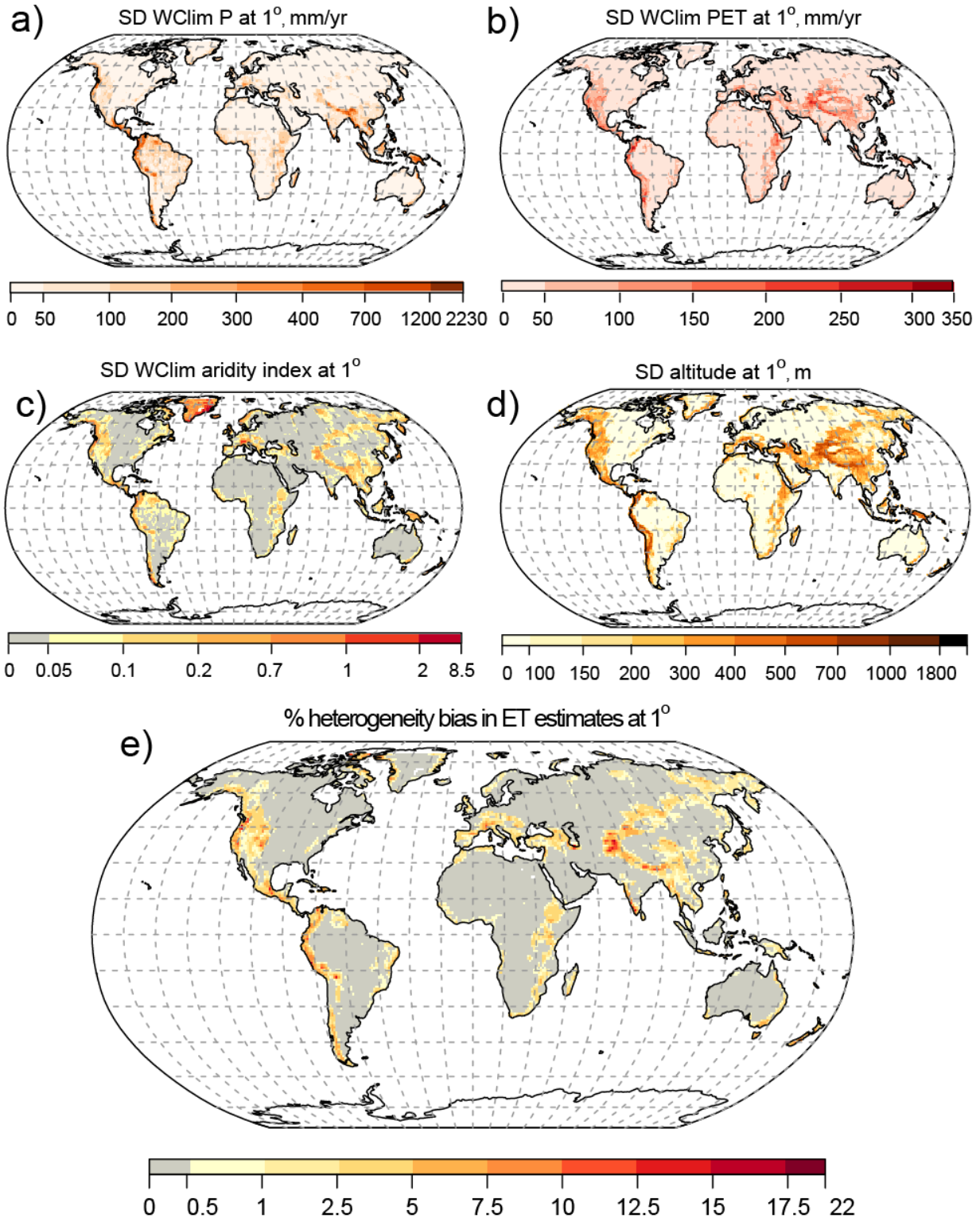
229

230 Our results show that the topographic gradient, and hence the variability in the aridity index across a given grid  
231 scale, drives consistent, predictable patterns of heterogeneity bias in evapotranspiration estimates at that scale.  
232 Equation 4 shows that this bias is equally sensitive to fractional variability in P and PET (standard deviation divided  
233 by mean). However, because P is typically more variable (in percentage terms) than PET across landscapes, the  
234 variability in P will usually make a larger contribution to the heterogeneity bias.





236  
 237 Figure 2. Global distribution of one-kilometer resolution annual mean precipitation (a: P; WorldClim; Hijmans et al.,  
 238 2005), potential evapotranspiration (b: PET; WorldClim; Hijmans et al., 2005), aridity index (c: AI=P/PET; WorldClim;  
 239 Hijmans et al., 2005), and topography (d: SRTM; Jarvis et al., 2008), along with (e) evapotranspiration (ET) at 1° by  
 240 1° scale by averaging 1km values of ET calculated using the Budyko function (Eq. 1).



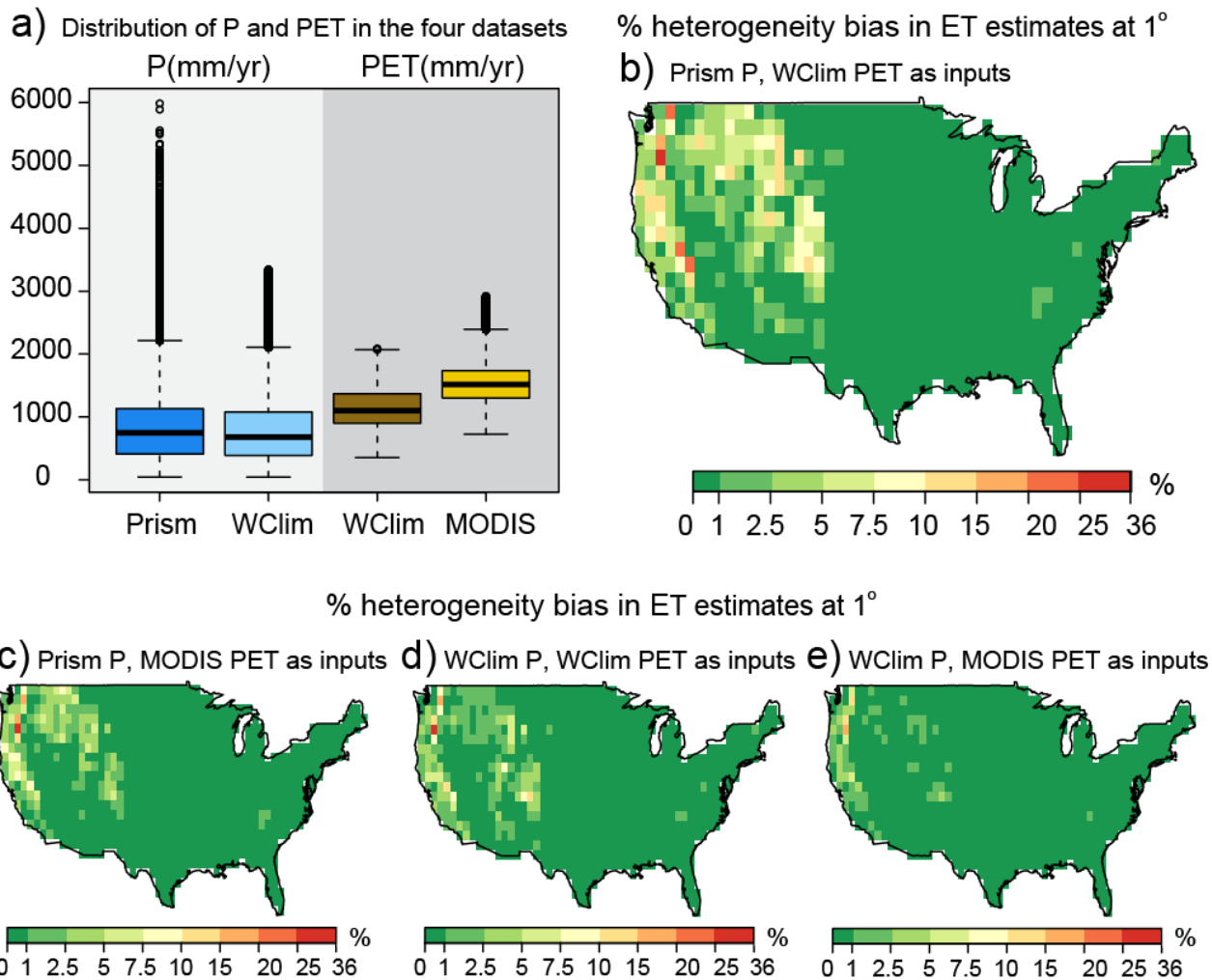
242  
 243 Figure 3. Global spatial distribution of variability (standard deviation) of one-kilometer values of a) precipitation (P),  
 244 b) potential evapotranspiration (PET), c) aridity index (AI=P/PET), and d) altitude at 1° by 1° grid cell. The  
 245 heterogeneity bias in ET estimates (e) is calculated using Eq. (4). Grid cells with larger standard deviation in altitude  
 246 and aridity index have larger heterogeneity bias.

#### 247 **4. Variation in heterogeneity bias across climate zones, data sources, and grid scales**

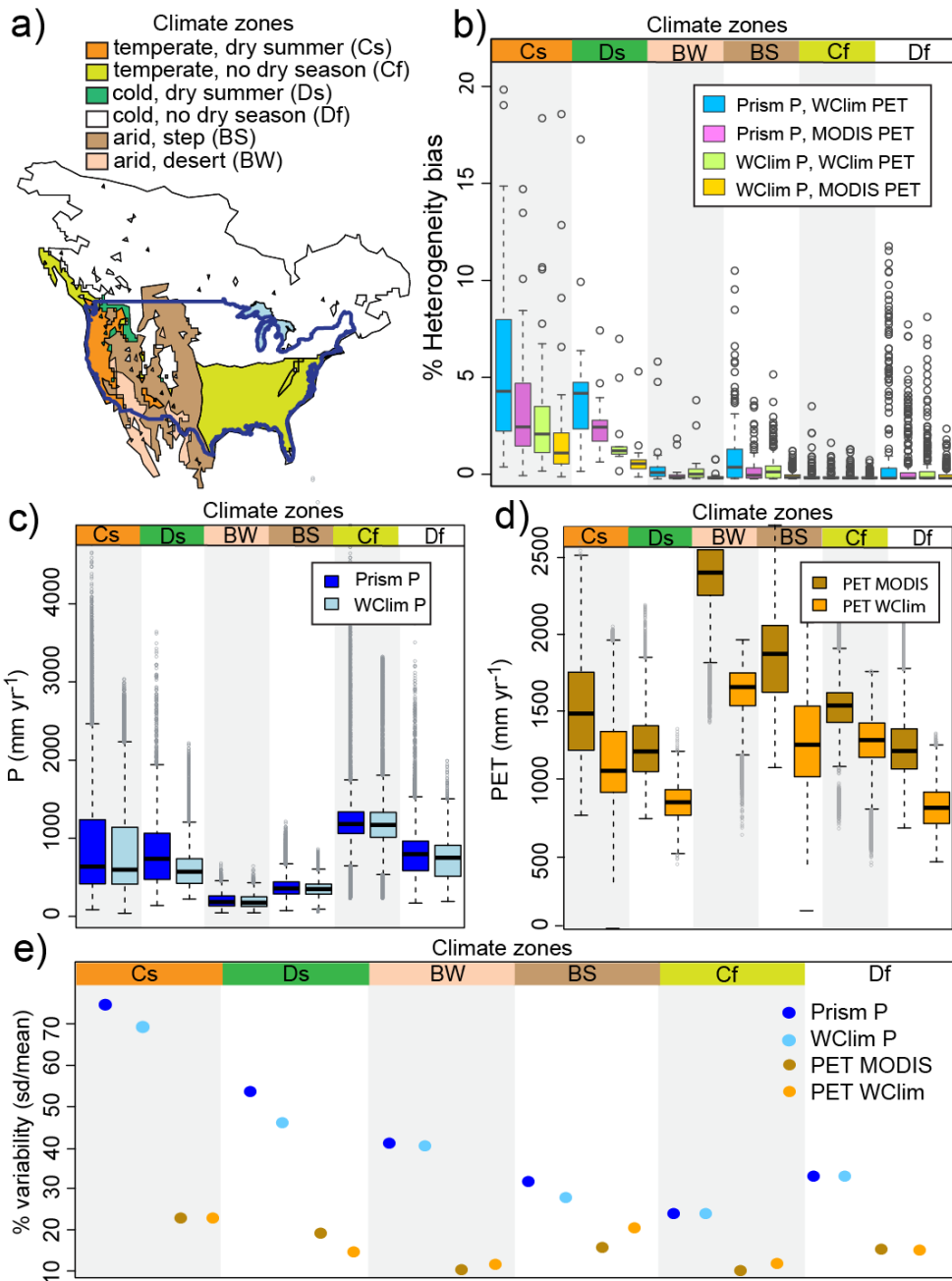
248 With increased availability of spatial data, it is becoming standard practice to assess input data uncertainties and  
249 their propagated impacts on water and energy flux estimates in land surface models. To quantify how choices  
250 among alternative input data products could affect the heterogeneity bias in ET estimates, we calculated the  
251 heterogeneity bias at 1° by 1° grid cell resolution across the contiguous US using four different pairs of P and PET  
252 data products. Two precipitation data sets, Prism (<http://prism.oregonstate.edu>) and WorldClim (Hijmans et al.,  
253 2005), along with two PET data sets, MODIS (Mu et al., 2007) and WorldClim (Hijmans et al., 2005), all at 1 km  
254 resolution, were combined in all possible pairs. The WorldClim PET dataset (Hijmans et al., 2005) is based on the  
255 Hargreaves method (Hargreaves and Samani 1985) while the MODIS PET product (Mu et al, 2007) is based on the  
256 Penman–Monteith equation (Monteith, 1965). The heterogeneity bias in ET estimates (Eq. 4), as outlined in Sect. 2,  
257 was evaluated from 1km values of P, PET, and the estimated average ET using the Budyko relationship (Eq. 1) for  
258 each of the four input data pairs. Figure 4a-e compares the spatial distributions of heterogeneity bias across the  
259 contiguous US for the four pairs of P and PET data products. The heterogeneity bias in ET estimates reached as high  
260 as 36 % in the western US using Prism P and WorldClim PET as input to the ET model (Fig. 4b). A visual comparison  
261 of Figs. 4b and Fig. 4d shows that the choice of P data source (Prism vs. WorldClim) had a bigger effect on the  
262 heterogeneity bias than the choice of PET data source (MODIS vs. WorldClim), meaning that the fractional  
263 variability in P is the dominant variable. In all cases, data sources that were more variable in relation to their means  
264 (Prism for P and WorldClim for PET; Fig. 4b) led to larger heterogeneity biases, as expected from Eq. (4). Thus we  
265 infer that we would have obtained larger heterogeneity biases if we had conducted our global analysis (Fig. 3) with  
266 Prism P and either WorldClim or MODIS PET, but we cannot show that result explicitly at global scale because Prism  
267 P is not freely available globally.

268  
269 If we separate the heterogeneity biases shown in Fig. 4 according to Köppen-Geiger climate zones (Peel et al., 2007;  
270 Fig. 5a), we see that they are distinctly higher in particular climate-terrain combinations. Heterogeneity biases are  
271 higher in regions with temperate climates and dry summers (climate zone Cs) and in regions with cold, dry  
272 summers (climate zone Ds), most likely due to the sharp spatial gradient in their water and energy sources for  
273 evapotranspiration (Fig. 5b). These areas typically have high topographic relief, combined with seasonal climate.  
274 The heterogeneity effects on ET estimates in these regions are expected to be even larger when a mechanistic  
275 model of ET is used. We expect that averaging over temporal variations of drivers of ET, especially in places with  
276 strong seasonality, could substantially bias the ET estimates, but this cannot be quantified in the Budyko framework  
277 due to its underlying steady-state assumptions. Figure 5b also illustrates the relative magnitudes of the  
278 heterogeneity biases obtained with the four pairs of P and PET data sources. The heterogeneity bias is the highest  
279 when the Prism P and WorldClim PET datasets are used, followed by the combination of Prism P and MODIS PET,  
280 which resulted in the second-highest heterogeneity bias across different climate zones. Equation 4 shows that  
281 heterogeneity biases in Budyko estimates of ET are equally sensitive to the same percentage variability in P and  
282 PET. Thus the degree of sensitivity, per se, to P and PET variations expressed in percentage terms is the same.

283 Although Figs. 5c and 5d give the visual impression that PET is more variable than P across climate zones and  
 284 between data sources, Fig. 5e shows that the fractional variability in P is systematically higher than PET, and it also  
 285 varies more across the climate zones and between the two data sets. Because P is typically more variable than PET  
 286 (in percentage terms) across landscapes, the variability in P will make a larger contribution to the heterogeneity  
 287 bias (Fig. 5e) in the Budyko approach. Whether this is true for more physically based ET estimates remains to be  
 288 seen. Analysis of percent variability of P and PET products shows that percent variabilities of precipitation products  
 289 are in general larger than PET products and hence contribute more to heterogeneity (Fig 5e). While the percent  
 290 variabilities of the two PET products are in the same range, the percent variability in Prism precipitation is slightly  
 291 larger than in WorldClim precipitation, in regions with dry summers (Cs and Ds climate zones in Fig. 5a).  
 292

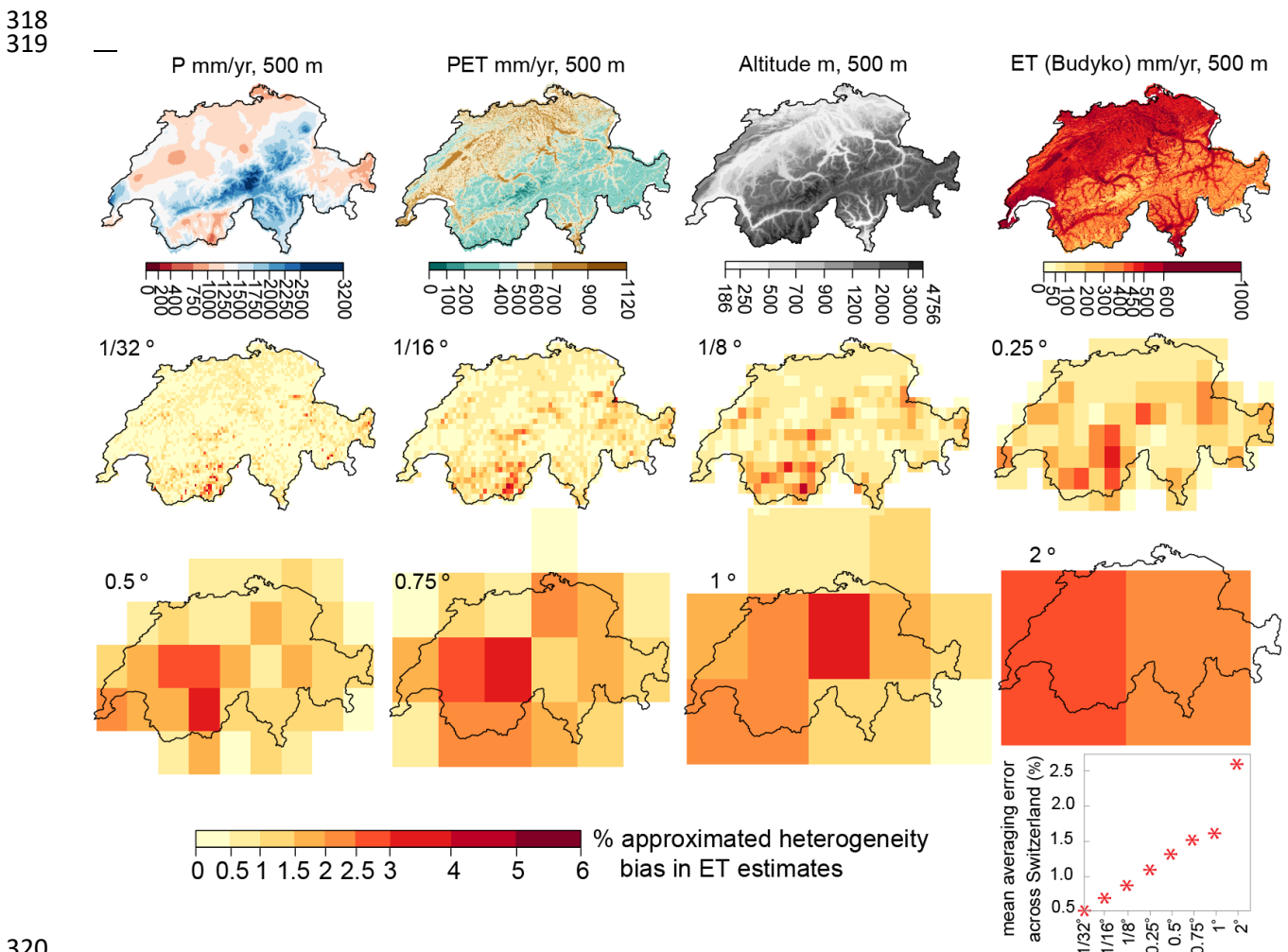


293  
 294 Figure 4. The distribution of P and PET in the four datasets is shown in a). Estimated heterogeneity bias (Eq. 4)  
 295 across the contiguous US using one-kilometer values of b) Prism P and WorldClim PET c) Prism P and MODIS PET d)  
 296 WorldClim P and WorldClim PET, and e) WorldClim P and MODIS PET as inputs.  
 297



298  
 299 Figure 5. a) Köppen-Geiger climate classification (Peel et al., 2007 in Beck et al. 2013) across the contiguous US, b)  
 300 the distribution of calculated heterogeneity bias in ET estimates (Eq. 4) at 1° by 1° grid cell in individual climate  
 301 zones, shown by boxplot (three data points with heterogeneity biases of over 20% are off-scale). Panels c and d  
 302 show the distribution of precipitation products (Prism and WorldClim) and potential evaporation products (MODIS  
 303 and WorldClim) at individual climate zones, respectively. The color-coded climate zones at the tops of panels b, c,  
 304 and d correspond to the climate zones mapped in panel a. Panel e compares the percentage variability of the two P  
 305 and PET data products across climate zones, showing that the percentage variability in P is markedly higher than in  
 306 PET, and the percentage variability in Prism P is somewhat higher than in WorldClim P, particularly in climate zones  
 307 with dry summers.

308 Because future increases in computing power will lead to ESMs with smaller grid cells, it is useful to ask how  
 309 changes in grid resolution affect the heterogeneity biases that we have estimated in this paper. To quantify the  
 310 heterogeneity bias in ET estimates as a function of grid scale, we repeated our analysis at various grid resolutions  
 311 using Switzerland as a test case. We started with high-resolution (500m) maps of long-term average annual  
 312 precipitation and PET across the Swiss landscape (Fig. 6), and then used Eq. 4 to estimate the heterogeneity bias at  
 313 grid scales ranging from  $1/32^\circ$  to  $2^\circ$  ( $\sim 3$  km to  $\sim 200$  km). As Fig. 6 shows, aggregating P and PET over larger scales  
 314 leads to larger, and more widespread, overestimates in ET. Conversely, at finer grid resolutions, the average  
 315 heterogeneity bias is smaller, and the locations with large biases are more localized. On average, the heterogeneity  
 316 bias across Switzerland as a whole grows exponentially as the inputs are averaged over larger grids (as shown in the  
 317 lower-right panel in Fig. 6).



320

321 Figure 6. Heterogeneity bias in ET estimates at various scales across Switzerland, estimated from 500m climate  
 322 data. ET is calculated using the Budyko relationship (Eq. 1). Heterogeneity bias was estimated from 500m  
 323 precipitation (P) and potential evapotranspiration (PET), and their variances at each grid scale, using Eq. 4. At finer  
 324 grid resolutions, the heterogeneity bias is more localized, and smaller on average.

325

## 326 5. Summary and discussion

327 Because evapotranspiration (ET) processes are inherently bounded by water and energy constraints, over the long  
328 term, ET is always a nonlinear function of available water and PET, whether this function is expressed as a Budyko  
329 curve or another ET model. These nonlinearities imply that spatial heterogeneity will not simply average out in  
330 predictions of land surface water and energy fluxes in ESMs. Overlooking sub-grid spatial heterogeneity in large-  
331 scale ESMs could lead to biases in estimated water and energy fluxes (e.g., ET rates). Here we have shown that,  
332 across several scales, averaging over spatially heterogeneous land surface properties and processes leads to biases  
333 in evapotranspiration estimates. Our analysis does not quantify the heterogeneity biases in ESMs, owing to the  
334 many differences between these mechanistic models and the simple empirical Budyko curve. But if the  
335 heterogeneity biases in ESMs can be quantified, they can be used as correction factors to improve ESM estimates of  
336 surface-atmosphere water and energy fluxes across landscapes. Our paper highlights a general methodology that  
337 can be used to estimate heterogeneity biases and to map their spatial patterns, but not to calculate their absolute  
338 magnitudes because those will change significantly depending on the ET formulation that is used.

339  
340 In this study, we used Budyko curves as simple models of ET, in which long-term average ET rates are functionally  
341 related to long-term averages of P and PET. We used an approach outlined by Rouholahnejad Freund and Kirchner  
342 (2017) to estimate the heterogeneity bias in modeled ET at 1-degree grid scale across the globe (Fig. 3), and also at  
343 multiple grid scales across Switzerland (Fig. 6), using finer-resolution P and PET values as drivers of ET. We showed  
344 how the heterogeneity effects on ET estimates vary with the nonlinearity in the governing equations and with the  
345 variability in land surface properties. Our analysis shows that heterogeneity effects on ET fluxes matter the most in  
346 areas with sharp gradients in the aridity index, which are in turn controlled by topographic gradients, and not  
347 merely in areas that are either arid or humid (e.g., compare Fig. 3e with Fig. 2c).

348  
349 According to our analysis, regions within the U.S. that have temperate climates and dry summers exhibit greater  
350 heterogeneity bias in ET estimates (Fig. 5). We show that the heterogeneity bias in ET estimates at each grid scale  
351 depends on the variance in the drivers of ET at that scale (Fig. 4), and on the choice of data sources used to  
352 estimate ET. Heterogeneity bias was significantly larger across the contiguous United States when P and PET data  
353 sources with larger variances were used (Fig. 4).

354  
355 We also explored the magnitude and spatial distribution of heterogeneity bias in ET estimates as a function of the  
356 scale at which the climatic drivers of ET are averaged. We found that as heterogeneous climatic variables are  
357 aggregated to larger scales, the heterogeneity biases in ET estimates become greater on average, and extend over  
358 larger areas (Fig. 6). At smaller grid scales, the heterogeneity bias does not completely disappear, but instead  
359 becomes more localized around areas with sharp topographic gradients. Finding an effective scale at which one can  
360 average over the heterogeneity of land surface properties and processes has been a longstanding problem in Earth  
361 science. Our analysis shows that at smaller resolutions the average heterogeneity bias as seen from the

362 atmosphere becomes smaller, but there is no characteristic scale at which it vanishes entirely (Fig. 6). The  
363 magnitude and spatial distribution of this bias depend strongly on the scale of the averaging and degree of the  
364 nonlinearity in the underlying processes. The heterogeneity bias concept is general and extendable to any convex  
365 or concave function (Rouholahnejad Freund and Kirchner 2017), meaning that in any nonlinear process, averaging  
366 over spatial and temporal heterogeneity can potentially lead to bias.

367  
368 One should keep in mind that the true mechanistic equations that determine point-scale ET as a function of point-  
369 scale water availability and PET (if such data were available) may be much more nonlinear than Budyko's empirical  
370 curves, because these curves already average over significant spatial and temporal heterogeneity. Thus, we expect  
371 that the real-world effects of sub-grid heterogeneity are probably larger than those we have estimated in Sects. 3  
372 and 4 of this study. In addition, the 1km P and PET values that are used in our global analysis might be still too  
373 coarse to represent small-scale heterogeneity that is important to evapotranspiration processes.

374  
375 Budyko curves are empirical relationships that functionally relate evaporation processes to the supply of water and  
376 energy under steady-state conditions in closed catchments with no changes in storage. Our analysis likewise  
377 assumes no changes in storage, nor any lateral transfer between the model grid cells, although both lateral  
378 transfers and changes in storage may be important, both in the real world and in models. Unlike the Budyko  
379 framework, ET fluxes in most ESMs are often physically based (not merely functions of P and PET) and are  
380 calculated at much smaller time steps (seconds to minutes). These models often represent more processes that are  
381 important to evapotranspiration (such as storage variations) and include their dynamics to the extent that is  
382 computationally feasible. Because these relationships may be much more nonlinear than Budyko curves, there may  
383 also be significant heterogeneity biases when complex physically based models are used to estimate ET from  
384 spatially aggregated data. Therefore, we are now working to quantify heterogeneity bias in ET fluxes using a more  
385 mechanistic land surface model.

386

### 387 **Acknowledgements**

388 E.R.F. acknowledges support from the Swiss National Science Foundation (SNSF) under Grant No. P2EZP2\_162279.  
389 The authors thank Massimiliano Zappa of the Swiss Federal Research Institute WSL for providing the 500m  
390 resolution data that enabled the analysis shown in Fig. 6.

391

### 392 **References**

393 Aminzadeh M., and D. Or: The complementary relationship between actual and potential evaporation for spatially  
394 heterogeneous surfaces, *Water Resour. Res.*, 53, 580–601, doi:10.1002/2016WR019759, 2017.



395 Avissar, R., R. A. Pielke: A Parameterization of Heterogeneous Land Surfaces for Atmospheric Numerical Models and  
396 Its Impact on Regional Meteorology, *Monthly Weather Review*, vol. 117, issue 10, p. 2113, doi:10.1175/1520-  
397 0493(1989)117<2113:APOHLS>2.0.CO;2, 1989.

398 Baker I. T. , P. J. Sellers , A. S. Denning, I. Medina , P. Kraus, K. D. Haynes , and S. C. Biraud: Closing the scale gap  
399 between land surface parameterizations and GCMs with a new scheme, SiB3-Bins, *Journal of Advances in Modeling*  
400 *Earth Systems*, *J. Adv. Model. Earth Syst.*, 9, 691–711, doi:10.1002/2016MS000764, 2017.

401 Bastiaanssen, W. G. M., M. Menenti, R. A. Feddes, and A. A. M. Holtslag: A remote sensing surface energy balance  
402 algorithm for land (SEBAL): 1. Formulation, *Journal of Hydrology*, 212-213, 198–212, 1998.

403 Beck H. E., A. I. J. M. van Dijk, D. G. Miralles, R. A. M. de Jeu, L. A. Bruijnzeel, T. R. McVicar, and J. Schellekens:  
404 Global patterns in base flow index and recession based on streamflow observations from 3394 catchments, *Water*  
405 *Resour. Res.*, 49, 7843–7863, doi:10.1002/2013WR013918, 2013.

406 Boone, A., and O. J. Wetzel: A simple scheme for modeling sub-grid soil texture variability for use in an atmospheric  
407 climate model. *Journal of the Meteorological Society of Japan*, 77(1), 317–333, 1998.

408 Budyko, M. I.: *Climate and life*, Academic, New York, 1974.

409 Clark, M. P., Y. Fan, D. M. Lawrence, J. C. Adam, D. Bolster, D. J. Gochis, R. P. Hooper, M. Kumar, L. R. Leung, D. S.  
410 Mackay, R. M. Maxwell, C. Shen, S. C. Swenson, and X. Zeng: Improving the representation of hydrologic processes  
411 in Earth System Models, *Water Resour. Res.*, 51, 5929–5956, doi:10.1002/2015WR017096, 2015.

412 Ershadi A., M. F. McCabe, J. P. Evans, J. P. Walker: Effects of spatial aggregation on the multi-scale estimation of  
413 evapotranspiration, *Remote Sensing of Environment* 131, 51–62, <http://dx.doi.org/10.1016/j.rse.2012.12.007>,  
414 2013.

415 Fan, Y., M. Clark, D. M. Lawrence, S. Swenson, L. E. Band, S. L. Brantley, P. D. Brooks, W. E. Dietrich, A. Flores, G.  
416 Grant, J. W. Kirchner, D. S. Mackay, J. J. McDonnell, P. C. D. Milly, P. L. Sullivan, C. Tague, H. Ajami, N. Chaney, A.  
417 Hartmann, P. Hazenberg, J. McNamara, J. Pelletier, J. Perket, E. Rouholahnejad-Freund, T. Wagener, X. Zeng, E.  
418 Beighley, J. Buzan, M. Huang, B. Livneh, B. P. Mohanty, B. Nijssen, M. Safeeq, C. Shen, W. van Verseveld, J. Volk, D.  
419 Yamazaki: Hillslope hydrology in global change research and Earth system modeling, *Water Resources Research*, 55,  
420 doi:10.1029/2018WR023903, 2019.

421 Giorgi, F., and R. Avissar: Representation of heterogeneity effects in Earth system modeling: Experience from land  
422 surface modeling, *Rev. Geophys.*, 35, 413–437, doi:10.1029/97RG01754, 1997.

423 Hargreaves, G. H., and Z. A. Samani: Reference crop evaporation from temperature, *Appl. Eng. Agric.*, 1(2), 96-99,  
424 1985.

425 Hijmans, R. J., S. E. Cameron, J. L. Parra, P. G. Jones, and A. Jarvis: Very high resolution interpolated climate surfaces  
426 for global land areas, *Int. J. Climatol.*, 25, 1965–1978, doi:10.1002/joc.1276, 2005.

427 Holland, S., J. L. Heitman, A. Howard, T. J. Sauer, W. Giese, A. Ben-Gal, N. Agam, D. Kool, and J. Havlin: Micro Bowen  
428 ratio system for measuring evapotranspiration in a vineyard interrow, *Agric. For. Meteorol.*, 177, 93–100, 2013.

429 Hong, S. H., J. M. H. Hendrickx, and B. Borchers: Up-scaling of SEBAL derived evapotranspiration maps from Landsat  
430 (30 m) to MODIS (250 m) scale, *Journal of Hydrology*, 370, 122–138, 2009.

431 Jarvis, A., Reuter, H. I., Nelson, A., and Guevara, E.: Hole-filled SRTM for the globe Version 4, available from the  
432 CGIARCSI SRTM 90m Database, <http://srtm.csi.cgiar.org> (last access: 26 February 2016), 2008.

433 Kalma, J. D., T. R. McVicar, and M. F. McCabe: Estimating land surface evaporation: A review of methods using  
434 remotely sensed surface temperature data, *Surv. Geophys.*, 29, 421–469, doi:10.1007/s10712-008-9037-z, 2008.

435 Kollet S. J.: Influence of soil heterogeneity on evapotranspiration under shallow water table conditions: transient,  
436 stochastic simulations, *Environmental Research Letters*, 4, 35007, doi:10.1088/1748-9326/4/3/035007, 2009.

437 Koster R. D. et al.: GLACE: The Global Land– Atmosphere Coupling Experiment. Part I: Overview. *J. Hydrometeorol.*, 7,  
438 590–610, 2006.

439 Koster R. D., and M. Suarez: Modeling the land surface boundary in climate models as a composite of independent  
440 vegetation stands, *J. Geophysical Research*, 97 (D3), 26-97-2715, 1992.

441 Lu, H., T., Liu, Y. Yang, D. Yao: A hybrid dual-Source model of estimating evapotranspiration over different  
442 ecosystems and implications for satellite-based approaches, *Remote Sens.* 6, 8359–8386, 2014.

443 Maayar, M. E., J. M. Chen: Spatial scaling of evapotranspiration as affected by heterogeneities in vegetation,  
444 topography, and soil texture, *Remote Sensing of Environment*, 102, 33–51, 2006.

445 Mahrt, L., J. Sun, D. Vickers, J. I. MacPherson, J. R. Perderson, and R. L. Desjardins: Observations of fluxes and inland  
446 breezes over a heterogeneous surface, *J. Atmos. Sci.* 51, 2165e2178, 1992.

447 McCabe M., and E. Wood: Scale influences on the remote estimation of evapotranspiration using multiple satellite  
448 sensors, *Remote Sensing of Environment* 105 (2006) 271–285, 2006.

449 Mezentsev, V. S.: More on the calculation of average total evaporation, *Meteorol. Gidrol.*, 5, 24–26, 1955.

450 Montheith, J. L.: Evaporation and environment, the state of and movement of water in living organisms, *Proceeding*  
451 *of Soc. for Exp. Biol.*, 19, 205-234, doi:10.1002/qj.49710745102, 1965.

452 Mu, Q., F. A. Heinsch, M. Zhao, and S. W. Running: Development of a global evapotranspiration algorithm based on  
453 MODIS and global meteorology data, *Remote Sens. Environ.*, 111, 519–536, doi:10.1016/j.rse.2007.04.015, 2007.

454 Peel, M. C., B. L. Finlayson, and T. A. McMahon: Updated world map of the Köppen-Geiger climate classification,  
455 Hydrol. Earth Syst. Sci., 11, 1633-1644, <https://doi.org/10.5194/hess-11-1633-2007>, 2007.

456 PRISM Climate Group, Oregon State University, <http://prism.oregonstate.edu>, created 22 Feb 2017.

457 Rouholahnejad Freund, E., and J. W. Kirchner: A Budyko framework for estimating how spatial heterogeneity and  
458 lateral moisture redistribution affect average evapotranspiration rates as seen from the atmosphere, Hydrology  
459 and Earth System Sciences, 21(1), 217-233, 2017.

460 Santanello J. R., and C. D. Peters-Lidard: Diagnosing the Sensitivity of Local Land–Atmosphere Coupling via the Soil  
461 Moisture–Boundary Layer Interaction, J. Hydrometeorology, 12, 766-786, doi: 10.1175/JHM-D-10-05014.1, 2011.

462 Sato N., P. J. Sellers, D. A. Randall, E. K. Schneider, J. Shukla, J. L. Kinter III, Y. T. Hou, and E. Albertazzi: Effects of  
463 Implementing the Simple Biosphere Model in a General Circulation Model, J. Atmospheric Sciences, 46(18), 2757-  
464 2782, 1989.

465 Seneviratne, S. I., T. Corti, E. L. Davin, M. Hirschi, E. B. Jaeger, I. Lehner, B. Orlowsky, and A. J. Teuling: Investigating  
466 soil moisture–climate interactions in a changing climate: A review, Earth-Science Reviews, 99(3–4), 125-161, 2010.

467 Shahraeeni, E., and D. Or: Thermo-evaporative fluxes from heterogeneous porous surfaces resolved by infrared  
468 thermography, Water Resour. Res., 46, W09511, doi:10.1029/2009WR008455, 2010.

469 Su, Z.: The Surface Energy Balance System (SEBS) for estimation of turbulent heat fluxes. Hydrology and Earth  
470 System Sciences, 6, 85–100, 2002.

471 Turc, L.: Le bilan d'eau des sols: relation entre la precipitations, l'évaporation et l'écoulement, Ann. Agron. A, 5,  
472 491–569, 1954.

473 Wood, N., and P. J. Mason: The influence of static stability on the effective roughness length for momentum and  
474 heat transfer, Quart. J. Roy. Meteor. Soc. 117, 1025e1056, 1991.